

# From pseudomorphic to orthomorphic growth of Fe films on Cu<sub>3</sub>Au(001).

F. Bruno,<sup>a</sup> S. Terreni,<sup>b</sup> L. Floreano,<sup>a</sup> D. Cvetko,<sup>a,c</sup> P. Luches,<sup>d</sup> L. Mattera,<sup>b</sup> A. Morgante,<sup>a,e</sup> R. Moroni,<sup>b</sup> A. Verdini,<sup>a</sup> and M. Canepa<sup>b,\*</sup>

<sup>a</sup>Laboratorio TASC dell'Istituto Nazionale per la Fisica della Materia, Trieste, Italy.

<sup>b</sup>INFN and Dipartimento di Fisica, Università di Genova,  
via Dodecaneso 33, I-16146 Genova, Italy

<sup>c</sup>J. Stefan Institute, University of Ljubljana, Slovenia, and Sincrotrone Trieste, Italy

<sup>d</sup>INFN and Dipartimento di Fisica, Università di Modena e Reggio Emilia, Modena, Italy. <sup>e</sup> Dipartimento di Fisica dell'Università di Trieste, Italy.

The structure of Fe films grown on the (001) surface of a Cu<sub>3</sub>Au single crystal at room temperature has been investigated by means of Grazing Incidence X-Ray Diffraction (GIXRD) and Photo/Auger–Electron Diffraction (ED) as a function of thickness in the 0–40 Å range. The combination of GIXRD and ED allows one to obtain quantitative information on the in–plane spacing  $a$  from the former technique, and the ratio between the vertical spacing  $c$  and  $a$ , from the latter one. At low coverage the film grows pseudomorphic to the face centered cubic substrate. The experimental results obtained on a film of 10 Å thickness clearly indicate the overcoming of the limit for pseudomorphic growth. Above this limit the film is characterized by the coexistence of the pseudomorphic phase with another tetragonally strained phase. Finally, above  $\sim 17$  Å the development of a body centered phase  $\alpha$ , whose unit cell is rotated of  $45^\circ$  with respect to the substrate one, has been clearly observed.  $\alpha$  is the dominating phase for film thickness above  $\sim 25$  Å and its lattice constant evolves towards the orthomorphic phase in strict quantitative agreement with epitaxial curves calculated for body centered tetragonal iron phases ( P.M. Marcus and F. Jona, Surf. Rev. and Lett. **1**, 15, 1994).

PACS: 68.55.-a; 68.55.Jk; 61.14.Qp

\* Corresponding author: Tel: \*\*39-010-3536287; Fax: \*\*39-010-311066;

E-mail address: canepa@fisica.unige.it; www.fisica.unige.it/surfmag

## INTRODUCTION

Very thin iron films, with physical properties at variance with the ordinary  $\alpha$ -Fe phase, can be grown on appropriately chosen substrates.<sup>1</sup> Such "artificial" phases represent an ideal ground in the investigation of the interplay between the structure and the magnetic properties of materials.<sup>2</sup> In this field, the  $\text{Cu}_3\text{Au}(001)$  surface has been considered as a candidate for the stabilisation of a face-centered-cubic (fcc), expanded volume, high-spin Fe phase.<sup>3</sup> For this substrate, a model of the so-called epitaxial lines of iron, calculated within the frame of linear elasticity theory, suggested the formation of a tetragonally strained phase, with some uncertainty on its body or face centered geometry.<sup>4</sup> The calculations did not consider interdiffusion processes between the Fe deposit and surface atoms, but both intermixing at the interface and substrate segregation have been reported for Fe deposited at room temperature (RT) on  $\text{Cu}(001)$ <sup>5</sup> and on  $\text{Au}(001)$ .<sup>6,7</sup>

In previous research on the magnetism of the  $\text{Fe}/\text{Cu}_3\text{Au}(001)$  films, three regions of thickness of different properties were identified.<sup>8-10</sup> At sub-monolayer coverage no hysteresis loops were detected. A second region was instead characterised by a magnetisation perpendicular to the surface. Then, at a critical thickness  $\Theta_{sw}$  of the order of a few monolayers and depending on the temperature of deposition, the magnetisation was found to switch to an in plane orientation (spin reorientation transition, in brief SRO) as in ordinary  $\alpha$ -Fe.

In spite of an overall agreement on film magnetism, no general consensus has been reached about the film structure. Regarding room temperature (RT) growth, an early LEED study claimed the occurrence of a face-centered cubic phase up to 7 Mono-Layers (ML).<sup>8</sup> In a more recent LEED I-V investigation the SRO transition ( $\Theta_{sw} \sim 4$  ML) was tightly related to a transition from an fcc to a bcc-like phase;<sup>9</sup> the LEED analysis was successively backed by an STM study in the coverage range of the SRO transition, pointing out a complex topography assigned to the coexistence of different phases.<sup>11</sup> Another LEED I-V study, backed by dynamical calculations, proposed instead a body-centered-tetragonal (bct) structure down to  $\Theta = 3.3$  ML with no apparent correlation between structural properties and the SRO transition.<sup>12</sup> Finally, in a recent electron scattering experiment (in the so-called Primary-beam Diffraction Modulated Electron Emission configuration, PDMEE)<sup>13</sup> an fcc-like structure was found for  $\Theta < 4$  ML; then in a region extending up to  $\approx 23$  ML, two different phases were detected. A unique phase of bct type was finally detected, at least within the outermost layers, for relatively thicker films, in agreement with results of Ref.<sup>12</sup>. Ref.<sup>13</sup> considered atomic exchange processes in some details, indicating the occurrence of a limited Au intermixing and segregation at the initial stages of growth.

The somewhat conflicting results demand for fur-

ther investigation. Here we report on experiments of  $\text{Fe}/\text{Cu}_3\text{Au}(001)$  RT growth performed at the ALOISA beamline at the Elettra Synchrotron (Trieste, Italy).<sup>14</sup> Our investigation deals with a structural characterization of films in a thickness range of 0-40 Å, performed by means of X-ray induced photo- (and/or Auger-) electron Diffraction (from now on ED for brevity) in the so-called forward scattering condition. In this condition, the emission intensity is enhanced along the direction of interatomic axes by means of a focusing effect.<sup>15</sup> The angular position of focusing peaks in polar ED scans is well known to provide "simple", chemically selected, short range information on the structure of the topmost layers of the films.<sup>16,17</sup> Furthermore, the availability of reliable calculations codes allows for a close comparison with experimental data and for quantitative analysis.<sup>18</sup>

In our experimental approach,<sup>19</sup> ED data are backed by Grazing Incidence X-Rays Diffraction (GIXRD) measurements, supplying information about the in-plane lattice parameter of films<sup>20</sup> and about the film morphology. In the next section details on the experimental procedures are reported. Experimental data will be described in sect. II. A quantitative analysis of the data can be found in the sect. III. A discussion of the results obtained follows in sect. IV. A summary and the conclusions can be found in sect. V.

## I. EXPERIMENTAL

The beamline ALOISA allows users to perform both electron spectroscopy and X-Ray surface diffraction measurements under the same experimental conditions.<sup>14,21</sup> The sample is mounted on a 6-degrees-of-freedom manipulator, specially designed to select with great accuracy ( $0.01^\circ$ ) the grazing angle of the beam electric field. The temperature of the sample, measured by thermocouples, can be varied by resistive heating and liquid nitrogen cooling. The UHV experimental chamber (base pressure in the  $10^{-11}$  mBar range) hosts the hemispherical electron analysers and X-Ray detectors. The emission direction from the sample surface can be freely selected for any orientation of the surface. For the surface preparation, the sample is translated in the preparation chamber (base pressure of  $1 - 2 \times 10^{-10}$  mBar) equipped with facilities for sputtering, evaporation cells, gas inlets and a RHEED system.

The surface preparation procedure was set up in previous He diffraction experiments.<sup>22,23</sup> The procedure takes into account the particular thermodynamics of  $\text{Cu}_3\text{Au}(001)$ , that is characterized by a continuous order/disorder (O/D) phase transition at the surface with a critical temperature  $T_c = 663$  K<sup>23</sup> and a bulk first order O/D transition at the same  $T_c$ .<sup>24</sup> An ordered surface, displaying sharp  $c(2 \times 2)$  RHEED patterns typical of the Au-Cu termination,<sup>25</sup> was obtained by sputtering and careful annealing procedures described in details

elsewhere.<sup>23</sup> The same sample was also used in a previous synchrotron experiment<sup>19</sup> and in the PDMEE experiment of ref.<sup>13</sup>.

At ALOISA, XPS surveys at grazing incidence (of the order of the critical angle) were used to check contamination of light adsorbates and Fe residuals after the sputtering removal of films. A preliminary ED characterization of the substrate, backed by multiple scattering calculations has been presented in a previous paper.<sup>19</sup> Simulations taking into account the geometry for the Au-Cu termination available in literature<sup>26</sup> were found to be in excellent agreement with experimental results.

Iron was evaporated from a carefully outgassed electron bombardment cell (Omicron). A quartz microbalance allowed to tune the deposition flux (typically of the order of 1 layer per minute) prior to the deposition on the sample. In the series of experiments presented in this paper, the film thickness was calibrated by X-ray reflectivity from the sample during and after deposition. Fig. 1 shows a typical deposition curve, measured at an incidence (tilt) angle  $\alpha_{in} = 8.25^\circ$  and a photon energy of 3500 eV during film deposition at room temperature. The interference between the waves reflected by the film-vacuum and the substrate-film interfaces yields an oscillatory evolution of the reflectivity as a function of the overlayer thickness. For the selected vertical momentum transfer  $k_z = 2\frac{E}{hc} \sin \alpha_{in}$ , identical phase conditions occur after a thickness increase of  $\Delta D = \frac{2\pi}{k_z} = 12.35 \text{ \AA}$ , thus leading to an accurate calibration of the deposition rate. In the sequence of experiments, Fe evaporation was stopped at different points of the deposition curve ensuring a high reproducibility of the amount of deposited material and a reliable estimate of the coverage.

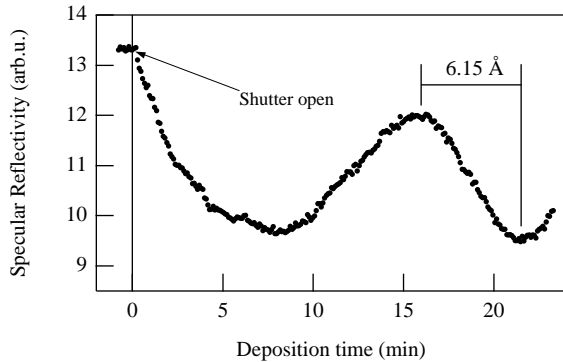


FIG. 1. X-Ray Specular Reflectivity taken during deposition at fixed energy (3500 eV) and grazing angle ( $8.25^\circ$ ). Maxima and minima arise from the interference between the interface and the growing film surface.

The post growth GIXRD measurements basically consisted of radial scans along the (200) position in the in-plane  $\text{Cu}_3\text{Au}(001)$  reciprocal lattice. These measurements were run scanning the photon energy in broad ranges under a suitable  $\theta$ - $2\theta$  scattering geometry. Both

the incidence angle of the beam and the emission angle were kept below the experimentally determined critical angle. The observation of diffraction peaks in radial scans allows to determine the in-plane spacing  $d$  through the Bragg condition  $2d \sin \theta = hc/E$ . Rocking curves of selected Bragg peaks, obtained by rotating the azimuthal angle at fixed energy, were measured to get additional information on the surface morphology.

A coverage estimate obtained by XPS measurements was found consistent with the reflectivity measurements within  $\pm 20\%$ . ED polar scans were measured by rotating the electron analyser in the plane defined by the surface normal and the beam axis, while keeping the grazing angle, the surface azimuthal orientation with respect to the beam axis and the polarization orientation fixed. We considered emission along  $\langle 100 \rangle_{sub}$  and  $\langle 110 \rangle_{sub}$ , the two main symmetry direction of the surface cell of the substrate. The photon energy was set to about 900 eV in order to look at several photoelectron and Auger peaks of Fe, Cu and Au. Here we will focus on the Fe  $L_{2,3}M_{23}M_{45}$  line at a K. E. of 698 eV. The signal was collected at the maximum and at suitably chosen energies aside the peak, in order to allow an effective subtraction of the background of secondaries.

## II. RESULTS

### A. GIXRD

In fig. 2, (H,0,0) radial scans taken on films of different thickness are shown. The pattern measured on the bare substrate is reported for comparison. In the measurements of fig. 2 the photon beam impinges the surface at grazing incidence, forming an angle  $\theta = 45^\circ$  with respect to the fcc(100) planes of the direct lattice.

Only a slight broadening of the  $(200)_{sub}$  peak of the substrate was observed at low coverage. A weak but fully detectable Fe-induced peak, indicated with  $\alpha'$  in fig. 2, was detected at  $\sim 10 \text{ \AA}$ , marking the first structural (and morphological) transition. The peak  $\alpha'$  becomes more intense in the 10-17  $\text{\AA}$  range. A shoulder appears at the left hand side of peak  $\alpha'$  at  $\Theta > 17 \text{ \AA}$ . For  $\Theta \geq 25 \text{ \AA}$  this shoulder develops in the well defined peak  $\alpha$ , that gradually moves away from the (200) reflection.

The position of the  $\alpha'$  peak in the 10  $\text{\AA}$  pattern of fig. 2,  $1.93 \pm 0.01$  r.l.u., corresponds to a distance  $d_{100} = 1.94 \pm 0.01 \text{ \AA}$  along the  $\langle 001 \rangle$  direction of direct space, eventually leading to a square cell of side  $a_{\alpha'} = d \cdot \sqrt{2} = 2.74 \pm 0.02 \text{ \AA}$ . This value can be compared with the lattice parameter of  $\text{Cu}_3\text{Au}(001)$  ( $a_{\text{CuAu}} = 2.65 \text{ \AA}$ ), with an estimate of  $a_{fcc} \sim 2.55 \text{ \AA}$  for an hypothetical fcc iron structure<sup>4</sup>, and with  $a_{bcc} = 2.87 \text{ \AA}$ , e.g the lattice parameter of a bcc film whose unit cell is rotated of  $45^\circ$  with respect to the fcc substrate (hereafter indicated as  $R^{45}bcc$ ).

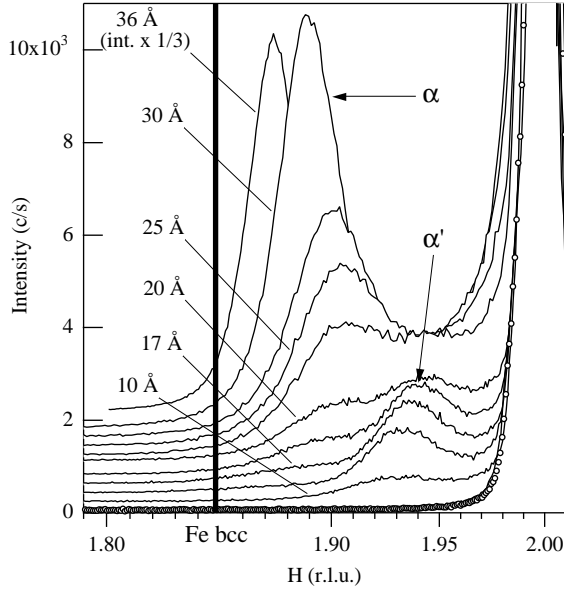


FIG. 2. In plane X-Ray Diffraction of the (2,0,0) diffraction peak taken at fixed scattering geometry by varying the photon energy. The data are shown as a function of the reciprocal lattice unit  $H$  of the  $fcc$   $Cu_3Au(100)$  substrate. Diffraction from the clean substrate is shown with open markers. Full lines are the diffraction measurements from Fe films at different thickness. The data have been vertically shifted by a constant offset (200 c/s) for the sake of clarity.

The position of the  $\alpha$  peak at 36 Å thickness in Fig. 2 corresponds to a lattice parameter  $a_\alpha = 2.830 \pm 0.005$  Å. The position of  $\alpha$  is indeed close to the (110) reflection of a  $R^{45}bcc$  structure. Further, reasonable arguments on the energetics of iron modifications and inspection of the so-called epitaxial lines calculated in ref.<sup>4</sup> led to consider the  $\alpha$  peak incompatible with an fct-like modification. The  $\alpha$  peaks were therefore assigned to tetragonally strained body centered ( $R^{45}bct$ ) structures.

The GIXRD measurements provided therefore valuable insight on the in-plane structure of the films; this information is relatively direct for those patterns presenting one dominant Fe-induced peak, as it is the case at very low (10 Å) and very large coverages (36 Å). In an intermediate region between 10 and 20 Å, the patterns are more complex, likely reflecting the coexistence of more than one phase in the film. A full structural determination requires also the value of the vertical lattice constant of the various iron phases which forms at different thickness. We extracted this information by ED, in the forward focusing regime.

## B. ED

ED polar scan measured on film of selected thickness for the Fe Auger line along the  $\langle 100 \rangle_{sub}$  and  $\langle 110 \rangle_{sub}$  directions, are reported in Figs. 3 and 4, respec-

tively. The patterns were obtained after subtraction of the background of secondaries. The peak F is originated by the forward scattering effect along off-normal nearest-neighbour chains. The position of this peak provides a guess on the ratio between the in-plane and vertical lattice constants of the film. In this respect, dotted and dashed lines in 3 and 4 mark the position of the F peak expected in case of  $fcc$  and  $R^{45}bcc$  geometry, respectively.

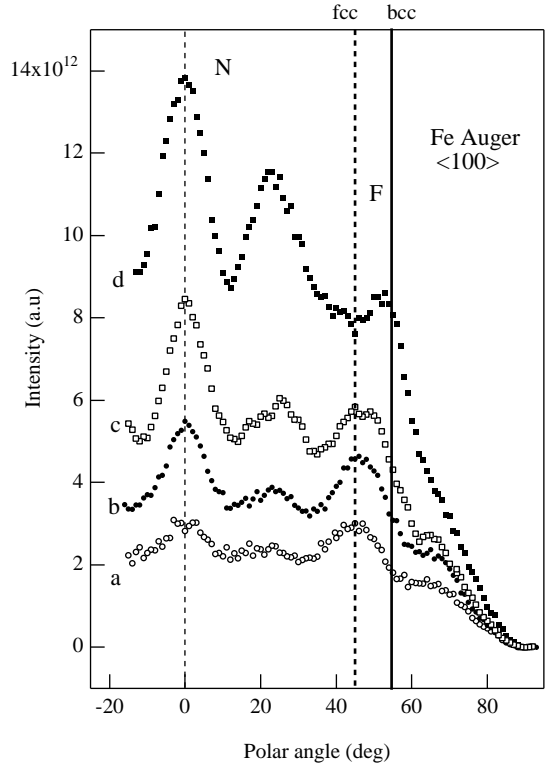


FIG. 3. Experimental Fe Auger LMM (K.E. = 698 eV) ED pattern along  $\langle 100 \rangle$  substrate symmetry direction for: a) the 3 Å film, b) the 10 Å film, c) the 20 Å film, d) the 36 Å film. The surface normal direction ( $N$ ) and the first neighbor direction ( $F$ ) are also indicated.

At the lowest coverage investigated ( patterns  $a$  of Figs. 3 and 4), the forward focusing peak  $F$  is fairly pronounced in the  $\langle 100 \rangle_{sub}$  scan close to the  $fcc$ -like position. The  $F$  peak lays close to the  $fcc$  marker in the  $\langle 110 \rangle_{sub}$  direction as well, though its intensity is very weak. Note in both patterns the presence of the forward focusing peak  $N$ , related to close-packed chains along the surface normal. At 10 Å ( pattern  $b$  of Figs. 3 and 4) the  $F$  peaks move slightly from the  $fcc$  markers towards larger polar angles. The angular shift of the  $F$  peaks becomes more evident at  $\Theta = 20$  Å ( patterns  $c$ ). Also the shape of the patterns shows evident variations with respect to lower coverages. In the spectra obtained on the film at  $\Theta = 36$  Å ( patterns  $d$ ), the  $F$  peak becomes narrower and shifts decisively towards the  $bcc$  position.

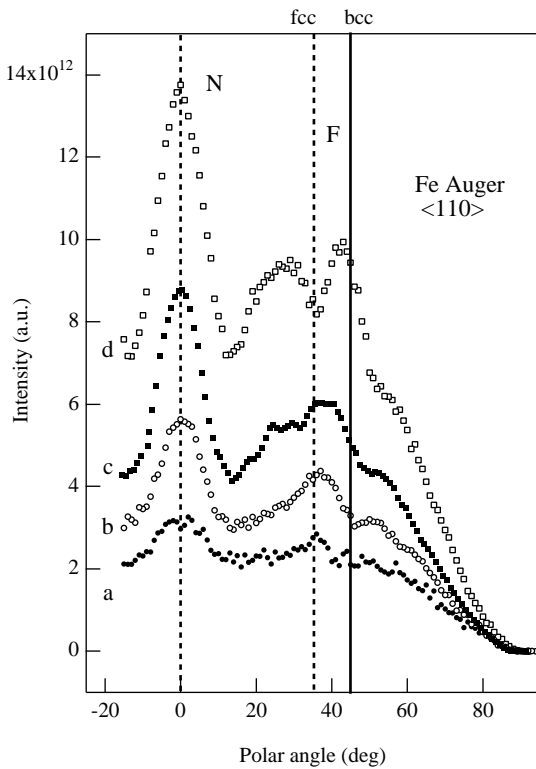


FIG. 4. Same of Fig. 3, but for the  $\langle 110 \rangle$  substrate symmetry direction. a) The 3 Å film, b) the 10 Å film, c) the 20 Å film, d) the 36 Å film.

We performed also ED measurements for the Auger lines of Cu and for the Au  $4f_{7/2}$  photoemission line. The experimental data resulted in overall agreement with results of ref.<sup>13</sup>, obtained on the same sample and under similar experimental conditions of this paper. We address the reader to Ref.<sup>13</sup> for a careful discussion of the intermixing between iron and substrate species.

### III. ED DATA ANALYSIS

In this section we present the structural models for the Fe film at different thickness, as obtained by comparison of the ED experimental data to multiple scattering calculations.

In our computational approach the ED polar pattern  $I_{exp}(\theta)$  is considered as a superposition of two contributions, according to the expression:

$$I_{exp}(\theta) = ISO_{exp}(\theta) \cdot (1 + \chi_{exp}(\theta)) \quad (1)$$

where  $ISO_{exp}(\theta)$  is a smooth, nearly isotropic background and the anisotropy term  $\chi_{exp}(\theta)$  is the diffractive part of the pattern, carrying the information on the interatomic distances.

The  $ISO_{exp}$  contribution is generally obtained by interpolating  $I_{exp}(\theta)$  to a polynomial and divided out in order to extract  $\chi_{exp}$ , which is then compared to calculated  $\chi_{calc}(\theta)$ <sup>27</sup>. We have preferred to afford a calculation

of the ISO term. Thus, the polar scans  $I_{exp}(\theta)$  have been compared with calculations:

$$I_{calc}(\theta) = ISO_{calc}(\theta) \cdot (1 + \chi_{calc}(\theta)) \quad (2)$$

For any given model the anisotropy term  $\chi_{calc}$  has been calculated by means of the MSCD code package<sup>28</sup>, while the ISO term has been written as the product of several factors.<sup>29,30</sup> First, an emission factor accounts for the electron emission matrix element;<sup>31</sup> it is determined by the polarization of the beam and by the initial and final states of the emitted electron. A second factor bears the information on the excited electron escape path through the Fe film;<sup>29</sup> it depends on the thickness and the homogeneity of the film. A third factor accounts for the surface roughness.<sup>32</sup> Finally, an instrumental factor accounts for the beam spot size on the sample and the angular acceptance of the detector. The calculation of the ISO part requires therefore reasonable estimates on the thickness and the surface roughness of the film and on the electronic mean free path.

Concerning MSCD calculations, the non structural input parameters, i.e. Multiple Scattering order = 6 and the inner potential = 10 eV have been fixed for all the simulations. Clusters of at least 180 atoms have been considered. The isotropic emission for the Auger electrons has been simulated by the transition from an initial  $p$ -level to an  $s$  ( $l-1$ ) final-state level.

The value of the lattice parameter of the in-plane square cell  $a$  has been obtained from the GIXRD measurement, while the ratio between the vertical spacing  $c$  and  $a$ , was first estimated by visual inspection of the angular position of the F peaks in the ED patterns. With these input parameters, the structural models have been refined by calculating  $\chi_{calc}(\theta)$  as a function of  $a$  and  $c$ .

#### A. Low Coverage: $\Theta < 10 \text{ \AA}$

The patterns of Figs. 3 and 4 force to consider an fcc-like structure. Although results from Ref.<sup>13,19</sup> suggested a limited degree of mixing of Au in the first few layers, a reasonable fitting of the data was possible disregarding atomic exchange processes.<sup>33</sup> The comparison between MSCD calculations and the experimental ED scans is reported in fig. 5. Note that the same  $ISO_{calc}(\theta)$  is used in both azimuthal directions.

The polar scans compare rather well (dashed lines) with a simple three-layer Fe pseudomorphic fcc film ( $a = 2.65 \text{ \AA}$ ;  $c/a = 1.41$ ) built on an unrelaxed substrate extending three layers beneath. However, a slightly better agreement (full lines in Fig. 5) was found by admitting a slight tetragonal distortion with  $a_\gamma = 2.65 \text{ \AA}$  and  $c/a_\gamma = 1.38$ .

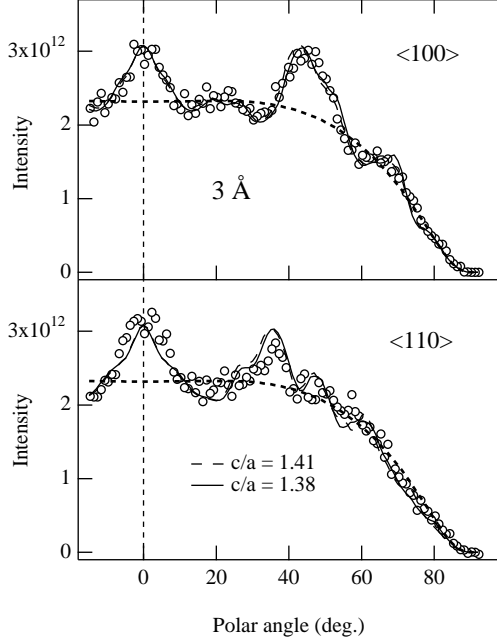


FIG. 5. Comparison of the ED data at 3 Å Fe thickness with a pseudomorphic model structure. Calculations are shown for both the unrelaxed ( $c/a_\gamma = 1.41$ , dashed line) and relaxed  $\gamma$  phase ( $c/a_\gamma = 1.38$ , full line). The same  $ISO_{catc}$  component, shown by heavy dashed lines, is used for both azimuthal directions

### B. Medium Coverage: $10 \text{ \AA} \leq \Theta \leq 20 \text{ \AA}$

The  $\alpha'$  peak in the GIXRD patterns at  $\Theta = 10 \text{ \AA}$  indicates a change of the growth mode. GIXRD and ED evidences can be rationalized if the coexistence of the two phases is assumed: the majority fcc-like phase, as seen at low coverage, is accompanied by the nucleation of a new phase  $\alpha'$ , minority phase at this stage.

The ED patterns have been compared to calculations performed on a crude model assuming the linear combination of two "independent" phases:

$$I_{th} = A \cdot I_\gamma + B \cdot I_{\alpha'}, \quad (3)$$

where

$$I_\gamma \rightarrow a_\gamma = 2.65 \text{ \AA} \text{ and } c/a_\gamma \sim 1.38$$

$I_{\alpha'} \rightarrow a_{\alpha'} = 2.74 \text{ \AA}$  (from GIXRD) and  $c/a_{\alpha'}$  to be determined.

$c/a_{\alpha'}$ ,  $A$  and  $B$  were varied in order to find the best agreement with experimental data. Taking into account the estimated thickness of the film, we have modelled a film of about 5-6 layers. A good agreement was obtained with  $c/a_{\alpha'} = 1.22$ ,  $A = 0.6$  and  $B = 0.4$  for both azimuthal directions (fig. 6).

For comparison, we also calculated the simulation for a homogeneous iron phase made of six complete layers, assuming the  $c/a$  ratio of 1.32 estimated by simple inspection of the angular position of the maximum of the

F peak in the polar pattern. This model yields a simulation of the ED data (not shown) definitely worse than the mixed phases model.

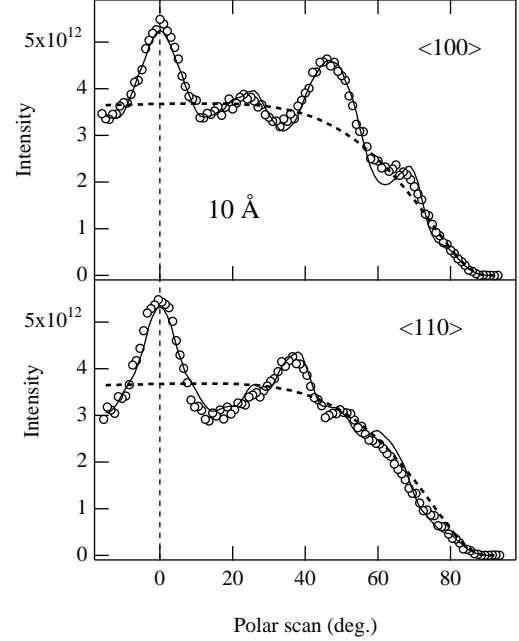


FIG. 6. Comparison of the ED data at 10 Å Fe thickness with calculations (full lines) based on a model which combines the  $\gamma$  and  $\alpha'$  phases. See text for the values of the lattice parameters and the weight of the phases. The same  $ISO_{catc}$  component, shown by heavy dashed lines, is used for both azimuthal directions

At 20 Å the F peaks are clearly shifted, indicating a change of the  $c/a$  ratio. Backed by GIXRD, a model considering the superposition of three phases was attempted:

$$I_{th} = A \cdot I_\gamma + B \cdot I_{\alpha'} + C \cdot I_\alpha \quad (4)$$

For simplicity, the parameters for the  $\gamma$  phase and the  $\alpha'$  phases were fixed at the same values found at lower coverage:

$$I_\gamma \rightarrow a_\gamma = 2.65 \text{ \AA}, c/a_\gamma \sim 1.38$$

$$I_{\alpha'} \rightarrow a_{\alpha'} = 2.74 \text{ \AA}, c/a_{\alpha'} = 1.22.$$

By taking  $A = 0.4$ ,  $B = 0.4$  and  $C = 0.2$ , a rather satisfactory agreement was found (fig. 7) with the following set of parameters for the phase  $\alpha$ ,

$$I_\alpha \rightarrow a_\alpha = 2.80 \text{ \AA}, c/a_\alpha = 1.05.$$

We note that a reasonable agreement was found also with a linear combination of the  $\gamma$  phase ( $a_\gamma = 2.65 \text{ \AA}$ ,  $c/a_\gamma \sim 1.38$ ) and the  $\alpha'$  phase ( $a_{\alpha'} = 2.74 \text{ \AA}$ ,  $c/a = 1.22$ ) found at 10 Å. However, in this case, we have found rather different values of the  $A$  and  $B$  coefficients along the two azimuthal directions considered. Finally, the simulation for a homogeneous phase model assuming  $c/a = 1.25$ , corresponding to the angular position of the F peak in the polar scan, gave a bad quality fit.

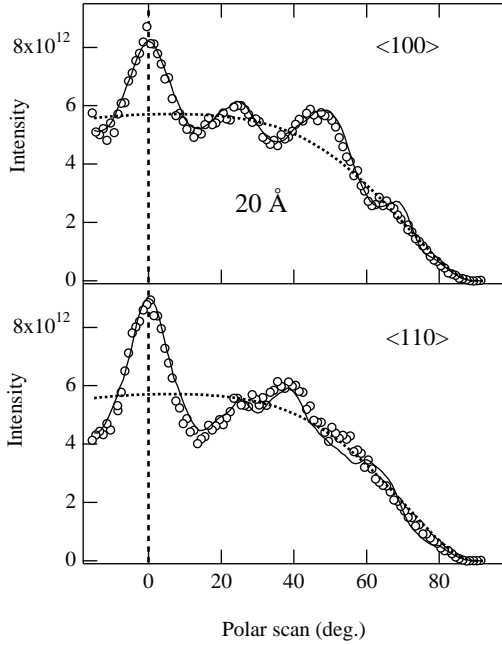


FIG. 7. Comparison of the ED data at 20 Å Fe thickness with calculations (full lines) based on a model which combines three phases ( $\gamma$ ,  $\alpha'$  and  $\alpha$ ). See text for the values of the lattice parameters and the weight of the phases. The same  $ISO_{calc}$  component, shown by heavy dashed lines, is used for both azimuthal directions.

### C. High Coverage: $\Theta > 25$ Å

The in-plane lattice parameter of the  $\alpha$  phase at 36 Å determined by GIXRD is  $a_\alpha = 2.830 \pm 0.005$  Å. The value of  $c/a_\alpha$  was determined by simulation of scattering from a free standing film consisting of a unique phase of 10 layers. The best fit yielded  $a_\alpha = 2.83$  Å and  $c/a_\alpha = 1.03 \pm 0.02$ . The best fit curves along  $\langle 100 \rangle_{sub}$  and  $\langle 110 \rangle_{sub}$  are reported (full lines) in Fig. 8. We found an excellent agreement along the  $\langle 110 \rangle_{sub}$  direction. The simulation reproduces rather accurately the angular position, intensity and width of the N and F peaks. The experimental data are not reproduced equally well along the  $\langle 100 \rangle_{sub}$  direction, possibly due to some morphological effect.<sup>34</sup> A similar analysis, performed on the film of 30 Å thickness provided  $a_\alpha = 2.810 \pm 0.005$  Å and  $c/a_\alpha = 1.05 \pm 0.02$ .

## IV. DISCUSSION

The single phase we found at the lower coverage represents the pseudomorphic phase predicted at initial stages of metal-on-metal epitaxy.<sup>35</sup> The thickness limit for pseudomorphic growth, marked by the appearance of the peak  $\alpha'$  in GIXRD measurements at  $\sim 10$  Å (for the pseudomorphic phase this corresponds to 5-6 ML), compares

well with the value obtained by a previous LEED I-V study.<sup>8</sup> The occurrence of a pseudomorphic  $\gamma$ -phase for lower coverage is also reported by other measurements on  $Cu_3Au(001)$ .<sup>9,13</sup> The thickness limit compares well also with a very recent determination on a related system as  $Fe/Cu_{90}Au_{10}(001)$ .<sup>36</sup> Minor discrepancies among the various papers probably reflect either the uncertainty in the coverage calibration or subtle differences in the growth procedures.

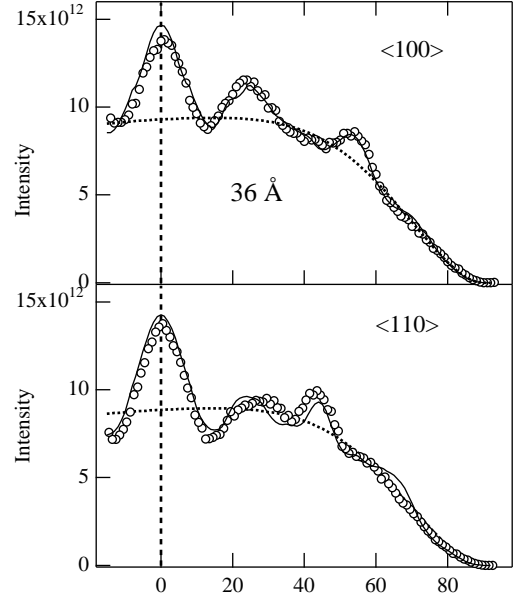


FIG. 8. Fits to the ED data at 36 Å Fe thickness with a body centered tetragonal model structure. The best fit (full lines) was obtained for  $a_\alpha = 2.83$  Å and  $c/a_\alpha = 1.03$ . The same  $ISO_{calc}$  component, shown by heavy dashed lines, is used for both azimuthal directions.

A relevant exception to such general agreement on initial stages of growth, is provided by the accurate analysis of Wuttig and coworkers.<sup>10,12</sup> In ref.<sup>12</sup>, LEED I-V measurements were compared with full dynamical calculations to determine the film structure at four different stages of growth. A single strained structure was proposed for films at 3.3 ML ( $\Theta$  about 5 Å,  $a = 2.72 \pm 0.06$  Å according to the data of table I of ref.<sup>12</sup>) and 4.8 ML ( $\Theta$  about 7 Å,  $a = 2.74 \pm 0.055$  Å). A bct character was assigned to this phase. However, in ref.<sup>12</sup> the authors deposited the first two layers at 150 K, while subsequent layers were post-deposited after heating at 300 K, so that the growth conditions could result significantly different from other works, particularly concerning a key factor such as intermixing. Concerning  $Fe/Cu_3Au$  growth at RT, a fraction of the order of 10% of a monolayer of Au atoms has been found to segregate for  $\Theta < 4$  ML.<sup>13</sup> An

Au concentration of a few percent has been also found within the Fe film.<sup>8,12,13</sup> The magnetic properties of the deposited film depend on the substrate temperature during deposition as well and appreciable deviations from the magnetic properties of RT grown films were obtained only a few degrees above RT.<sup>37</sup> We can then speculate that Cu and Au “impurities” or even some Au segregation at the surface of the film,<sup>13</sup> have some influence on the growth modes, probably contributing to the stabilization of the pseudomorphic phase.

The film evolution in the 10-20 Å coverage range seems rather intricate. In this respect, our data represent another example of the transition from the pseudomorphic to the orthomorphic phase involving rather complex paths depending on film temperature, thickness and degree of misfit.<sup>38,39</sup> Above  $\Theta \sim 10$  Å a single phase is no longer sufficient to explain the experimental data. This finding is fully consistent with Ref.<sup>13</sup> where two phases were clearly appreciable in the PDME patterns above 8 Å and with findings of ref.<sup>9</sup> and<sup>11</sup>. In this study we point out that up to three phases are necessary to rationalize GIXRD data and ED patterns close to 20 Å thickness. The analysis of previous section show that both the  $\alpha'$  and the  $\alpha$  phase are strained phases. The lattice parameters of the phase  $a_{\alpha'}$  ( $a_{\alpha'} = 2.74 \pm 0.02$  Å,  $c/a_{\alpha'} = 1.22 \pm 0.02$ ) do not match epitaxial lines calculated for bct and fct *bulk* modifications.<sup>4</sup> Information on this thickness range in the previous investigations was indeed rather scarce. A rough surface topography with “irregular” patches, was observed in STM pictures<sup>11</sup> for RT growth of 5 ML. This complex morphology pattern likely gives rise to the deterioration of electron diffraction patterns<sup>8,13</sup> generally observed in this range of coverage.

The “asymptotic” orthomorphic  $\alpha$  phase is clearly seen to develop around 25 Å in GIXRD patterns. In Fig. 9, we report the comparison of our results and the other experimental data available in literature for thick films with the theoretical prediction for the structure of bct phases, the so called epitaxial curves<sup>4</sup>. The full circles represent our structural determination for two films of 30 and 36 Å thickness. The circles represent the determinations of ref.<sup>12</sup> for a 18 and a 53 ML film. The triangle and the square represent the measurement of ref.<sup>13</sup> at 37 ML and that of ref.<sup>8</sup> for a 250 ML film, respectively. Our determination is in excellent agreement with calculations, thus confirming the interpretation advanced in ref.<sup>12</sup> for the  $\alpha$  phase.

The width of the  $\alpha$  peak bears information on the morphology of the phase. Profiles of the  $R_{45}^{bct}$  (110) and  $R_{45}^{bct}$  (100) peaks, obtained with an azimuthal scan at fixed energy (not shown), allowed an estimate of  $\sim 150$  Å for the domain size of the  $\alpha$  phase. The film at 36 Å is thus characterized by a significant amount of morphological disorder. In this respect, it is worth noting that homoepitaxial growth of Fe on Fe(001) at RT, in absence of surfactant species, proceeds in a three-dimensional fashion<sup>40,41</sup>, resulting in the formation of pyramidal mound-like structures.<sup>42</sup>

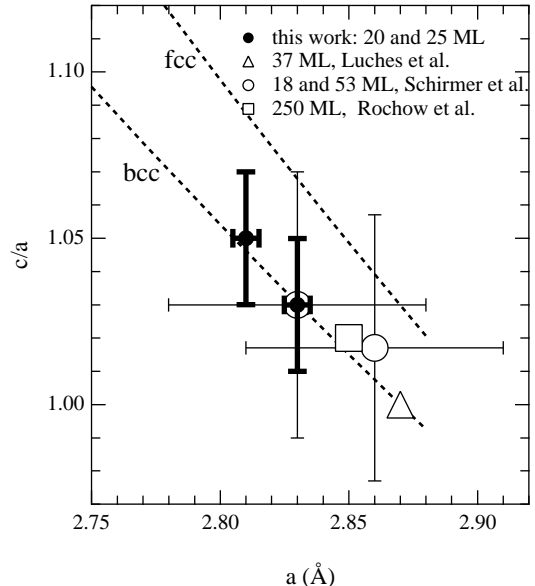


FIG. 9. Comparison of our results and other experimental data available in literature for thick films with the theoretical prediction for the structure of bct phases, the so called epitaxial curves [4]. The full circles represent our structural determination for two films of 30 and 36 Å thickness (corresponding to 20 and 25 ML, respectively). The circles represent the determinations of Ref. [12] for a 18 and a 53 ML film. The triangle and the square represent the measurement of Ref. [13] at 37 ML and that of Ref. [8] for a 250 ML film, respectively

The structure of the  $\alpha$  phase gradually changes as its thickness increases. It remains unclear whether the  $\alpha$  phase nucleates on top of inner “buffer” layers, working as adapters between the lattice parameter of the substrate and of the Fe bcc phase, or if its growth occurs at some expense of the inner phases, in particular of the  $\alpha'$  phase. The coexistence of the  $\alpha$  and  $\alpha'$  phases suggests a stacking of the two phases at some stage of growth.

## V. CONCLUSIONS

We have presented a combined GIXRD-ED study of the growth of thin films of Fe on Cu<sub>3</sub>Au(001). We observed the formation of different phases as a function of the film thickness. The main conclusions of this investigation can be summarized as follows:

- i. A single pseudomorphic phase of nearly fcc character ( $\gamma$ -phase) was observed well below 10 Å thickness. This conclusion is consistent with most of the previous works in literature<sup>3,8,9,13</sup> whereas it seems in apparent contrast with the analysis of ref.<sup>12</sup> that reports a bct phase down to  $\sim 5$  Å. In this respect, we suggested that exchange processes at the interface<sup>13</sup> can concur to the stabilization of the  $\gamma$  phase and we speculate that the different

results of ref.<sup>12</sup> are due to a lower influence of intermixing obtained during the deposition of the first two layers at 150 K.

ii. on a 10 Å thickness film, a neat Fe induced peak, clearly illustrating the overcoming of the thickness limit for pseudomorphic growth has been observed in the in-plane GIXRD measurements. Above this limit the film is characterized by the coexistence of phases: the  $\gamma$ -like pseudomorphic phase, most likely in inner layers, and a second strained phase  $\alpha'$ .

iii. Above 17 Å, we clearly observed the nucleation of a third strained phase,  $\alpha$ , which becomes the dominating structure above 25 Å. The  $\alpha$  phase is characterized by a body centered, tetragonally strained structure, whose unit cell is rotated of 45° with respect to the fcc substrate. The strain is progressively relieved with the increasing film thickness, in close agreement with the results of ref.<sup>12</sup>. The experimentally determined lattice constants of  $\alpha$  are in strict quantitative agreement with the epitaxial curves calculated in ref.<sup>4</sup>.

The combination of GIXRD and ED (backed by simulations of spectra) allowed us to obtain quantitative information on the geometric structures of phases. This information turned out to be very accurate in those regions of coverage where one phase is clearly dominant, as it is the case at very low (below 10 Å) and large coverages ( $> 30$  Å). A clear picture of the film morphology, specially when several phases coexist, is still an open issue, which require further investigations, specially with imaging techniques.

## ACKNOWLEDGEMENTS

Maurizio Canepa, Silvana Terreni and Lorenzo Mattera are very grateful to Fernando Tommasini for his continuous support to this experiment. The authors are then grateful to P. Cantini, G. Boato, S. Valeri and A. Di Bona for stimulating discussions on the Fe/Cu<sub>3</sub>Au system. The authors thank G. Gazzadi for discussions on the MSCD calculations and C. Mannori, S. Prandi and M. Repetto for helpful assistance at various stages of the experiment.

Funding from INFM and from the Italian Ministero dell'Università e Ricerca Scientifica (Cofin 990211848) are gratefully acknowledged.

<sup>1</sup> M. Wuttig, B. Feldmann, T. Flores, Surf. Sci. 331-333, 659 (1995).

<sup>2</sup> V.L. Moruzzi, P.M. Marcus, and J. Kübler, Phys. Rev. B **39**, 6957 (1989); P.M. Marcus, V.L. Moruzzi, S.-Q. Qiu, Phys. Rev. B **60**, 369 (1999).

- <sup>3</sup> S.H. Lu, J. Quinn, D. Tian, F. Jona and P.M. Marcus, Surf. Sci. **209**, 364 (1989).
- <sup>4</sup> P.M. Marcus and F. Jona, Surf. Rev. and Lett. **1**, 15 (1994).
- <sup>5</sup> D.D. Chambliss, R.J. Wilson and S. Chiang, J. Vac. Sci. Technol. A **10** (1992) 1993; M.T. Kief, J.W. Egelhoff, Phys. Rev. B **7**, 10785 (1993).
- <sup>6</sup> R. Opitz, S. Löbus, A. Thissen and R. Courths, Surf. Sci. **370**, 293 (1997).
- <sup>7</sup> O.S. Hernan, A.L. Vazquez de Parga, J.M. Gallego and R. Miranda, Surf. Sci. **415**, 106 (1998).
- <sup>8</sup> R. Rochow, C. Carbone, Th. Dodt, F.P. Johnen, and E. Kisker, Phys. Rev. B **41**, 3426 (1990).
- <sup>9</sup> M.-T. Lin, J. Shen, W. Kuch, H. Jenniches, M. Klaua, C.M. Schneider and J. Kirschner, Phys. Rev. B. **55**, 5886 (1997).
- <sup>10</sup> B. Feldmann, B. Schirmer, A. Sokoll and M. Wuttig, Phys. Rev. B. **57**, 1014 (1998).
- <sup>11</sup> M.-T. Lin, J. Shen, W. Kuch, H. jenniches, M. Klaua, C.M. Schneider and J. Kirschner, Surf. Sci. **410** (1998) 290.
- <sup>12</sup> B. Schirmer, B. Feldmann and M. Wuttig, Phys. Rev. B. **58** (1998) 4984.
- <sup>13</sup> P. Luches, A. Di Bona, S. Valeri, M. Canepa, Surf. Sci. **471**, 32 (2000).
- <sup>14</sup> An updated presentation of the beamline can be found at <http://tasc.area.trieste.it/tasc/lds/aloisa/aloisa.html>.
- <sup>15</sup> S. Kono, S.M. Goldberg, N.F.T. Hall, C.S. Fadley, Phys. Rev. Lett. **41**, 1831 (1978).
- <sup>16</sup> C.S. Fadley, *The Study of Surface Structures by Photoelectron Diffraction and Auger Electron Diffraction in Synchrotron Radiation research: Advances in Surface and Interface Science, Vol. 1: Techniques*, edited by R. Z. Bachrach, Plenum Press, New York, (1992), and references therein.
- <sup>17</sup> W.F. Egelhoff jr. in Ultrathin Magnetic Structures I, J.A.C.Bland and B. Heinrich eds., chapt. 5.1, p. 220, Springer - Verlag, Berlin 1994.
- <sup>18</sup> Y. Chen, F.J. Garcia de Abajo, A. Chassé, R.X. Ynzunza, A.P. Kaduwela, M.A. Van Hove and C.S. Fadley Phys. Rev. B **58**, 13121 (1998).
- <sup>19</sup> F. Bruno, D. Cvetko, L. Floreano, R. Gotter, C. Mannori, L. Mattera, R. Moroni, S. Prandi, S. Terreni, A. Verdini, M. Canepa, Appl. Surf. Sci. **162-163**, 340 (2000).
- <sup>20</sup> B.M. Lairson, A.P. Payne, S. Brennan, N.M. Rensing, B.J. Daniels, B.M. Clemens, J. Appl. Phys. **78**, 4449 (1995).
- <sup>21</sup> L. Floreano, G. Naletto, D. Cvetko, R. Gotter, M. Malvezzi, L. Marassi, A. Morgante, A. Santaniello, A. Verdini, F. Tommasini and G. Tondello Rev. of Sci. Inst. **70**, 3855 (1999).
- <sup>22</sup> C. Mannori, T. Scimia, P. Cantini, S. Terreni, M. Canepa, L. Mattera, Surf. Sci., **433**, 307 (1999).
- <sup>23</sup> C. Mannori, G. Boato, M. Canepa, P. Cantini, L. Mattera, S. Terreni, Europhysics Letters **45**, 686 (1999).
- <sup>24</sup> For a review, see Dosch H., Critical Phenomena at surfaces and interfaces, Springer Tracts Mod. Phys., vol. 126 (Springer, Berlin) 1992.
- <sup>25</sup> E.G. McRae and R. Malic, Surf. Sci. **148**, 551 (1984).
- <sup>26</sup> W.E. Wallace, G.J. Auckland, Surf. Sci. Lett. **275**, L685, (1992).
- <sup>27</sup> G.C. Gazzadi, P. Luches, A. Di Bona, L. Marassi, L. Pasquali, S. Valeri, S. Nannarone, Phys. Rev. B **61**, 2246

- (2000).
- <sup>28</sup> <http://electron.lbl.gov/mscdpack/mscdpack.html>. Further information can be found in *MSCD Package User Guide - Simulation of Photoelectron Diffraction using Rehr-Albers Separable Representation* by Y. Chen, M.A. Van Hove, handed out at *Trieste School on Use of Synchrotron Radiation, November 1997*.
- <sup>29</sup> C.S. Fadley *Basics Concepts of X-Ray Photoelectron Spectroscopy* in *Electron Spectroscopy, Theory, Techniques and Applications*, C.R.Brundle and A.D.Baker Eds. (Pergamon Press,1978), Volume II, Chapter 1.
- <sup>30</sup> F. Bruno, PhD. Thesis "Growth Methods at ALOISA", November 2000, University of Trieste.
- <sup>31</sup> J.W. Cooper, Phys. Rev. A **47**, 1841 (1993).
- <sup>32</sup> A.V. Yakovenko, J. Electron Spectroscopy and Relat. Phenom. **74**, 237 (1995).
- <sup>33</sup> The substrate temperature proved to be a very critical parameter in determining the level of Au surface segregation. In fact, the higher Au concentration at the Fe film surface, we found in the preliminary experiments [Ref. ASS], was associated with a slightly higher (15 -20 °C) substrate temperature during deposition.
- <sup>34</sup> Y. Park, E. E. Fullerton, S.D. Bader, Appl. Phys. Lett. **66**, 2140 (1995).
- <sup>35</sup> J.H. Van Der Merwe, J. Appl. Phys. **34**, 117 (1963).
- <sup>36</sup> S.S. Kang, W. Kuch, J. Kirschner, Phys. Rev. B **63**, 024401 (2000).
- <sup>37</sup> D. Tillmann and E. Kisker, Solid State Comm.**100**, 415 (1996).
- <sup>38</sup> W. Schindler et al. Surf. Sci. **465** , L783 (2000).
- <sup>39</sup> A. Biedermann, M. Schmid, P. Varga, Phys. Rev. Lett., **86** , 464 (2001).
- <sup>40</sup> J.A. Stroschio, D.T. Pierce, R.A. Dragoset, Phys. Rev. Lett. **70** , 3615 (1993).
- <sup>41</sup> P. Bonanno, M. Canepa, P. Cantini, L. Mattera, R. Moroni, S. Terreni, Surf. Sci. **454-456**,697 (2000).
- <sup>42</sup> K. Thürmer, R. Koch, M. Weber, K.H. Rieder, Phys. Rev. Lett. **75** 1767, (1995).